UNITED NATIONS EDUCATIONAL, SCIENTIFIC AND CULTURAL ORGANIZATION
INTERNATIONAL CENTRE FOR THEORETICAL PHYSICS
I.C.T.P., P.O. BOX 586, 34100 TRIESTE, ITALY, CABLE: CENTRATOM TRIESTE

H4.SMR/782-16

Second Workshop on
Three-Dimensional Modelling of Seismic Waves
Generation, Propagation and their Inversion

7 - 18 November 1994

Rayleigh Wave Group Velocity Tomography of Siberia, China and Vicinity

F.T. Wu* - A. Levshin**

* State University of New York
Department of Geological Sciences
Binghamton, New York
U.S.A.

**University of Colorado
Department of Physics
Boulder, Colorado
U.S.A.

II

Rayleigh Wave Group Velocity Tomography of Siberia, China and the Vicinity

Francis T. Wu

Department of Geological Sciences
State University of New York
Binghamton, New York 13902-6000

Anatoli L. Levshin

Joint Seismic Program Center
Department of Physics
University of Colorado
Boulder, Colorado 80309-0583

Vladmir M. Kozhevnikov

Institute of Earth Crust
Russian Academy of Sciences
Irkutsk, Russia

Abstract

Rayleigh waves are used in a tomographic inversion to obtain group velocity maps of East Asia ($40°E-160°E$ and $20°N-70°N$). The period range studied is 30 to 70 seconds. From these group velocity maps, average dispersion curves at twelve locations were determined and inverted to obtain velocity structures. Seismograms used for this study were recorded at CDSN stations, at a temporary array in Tibet, at several SRO stations, and stations established in Asia by the former Soviet Union, in Siberia, in the Sakhalin and in Mongolia. Altogether more than 1200 paths were available in the tomographic inversion. The study area includes the geologically ancient core of Asia, the Angara craton, around which the Asian continent accreted, the Altaids, a Paleozoic collision complex, Sino-Korean platform, a chain of Archaen terranes separated by belts of active structures, the south China platform, a collage of PreCambrain, Paleozoic and Mesozoic metamorphic and igneous terranes, as well as the Tibetan plateau, an active tectonic feature created in late Cenozoic through collision of the Indian subcontinent and the Asian continent. In the tomographic images, Tibet appears as a prominent low velocity (about -15% from the average) structure, with western and central Tibet often appear as the areas with the lowest velocities, the western Siberian platform, a part of the Altaids, and the Angara craton are consistently high group velocity areas. Many lesser tectonic features are recognizable in the tomographic images. Lake Baikal is seen as a high velocity feature at periods greater than 40 seconds. However, the high group velocity feature does not stop near the southern end of Lake Baikal; it extends south-southwestward across Mongolia. The North China Plain, a part of the platform where extensional tectonics dominates, is an area of high velocities as a result of relatively thin crust. The south China block, the least tectonically active region of China, is generally an area of high velocity. For periods

longer than 40 seconds, a NNE trending high group velocity gradient clearly exists in eastern China; the velocities are noticeably higher in the east. Main results of group velocity inversion include: (1) a Tibetan crust of around 60 km thick, with low crustal and upper mantle shear velocities, at 3.3 km/sec and 4.2 km/sec, respectively; (2) a crust of 33 km and a velocity of 4.58 in the western Siberian platform area; (3) a relatively thin crust under the Angara craton, but the upper mantle velocity is high at 4.58 km/sec. In many parts of the study area, where PreCambrian basement is exposed, the processes in the crust and upper mantle due to recent tectonic activities have modified the crust and upper mantle velocity structures under the PreCambrian terranes; they are no longer underlain by high velocity crust and mantle.

Introduction

The purpose of this study is to investigate the lateral variations of crust and upper mantle seismic velocity structures in Siberia, China and their vicinity. Rayleigh wave group velocity is chosen as datum because it is relatively easy to obtain a dense distribution of paths using the events in and on the periphery of the study area and the seismic stations internal to the study area. By combining data from the recently established high quality Chinese Digital Seismic Network (CDSN) stations and the upgraded Seismic Research Observatory (SRO) stations, data from a temporary network in Tibet, and a collection of data recorded at stations established by the former Soviet Union in Russia and Mongolia, we are able to obtain dispersion curves along more than 1200 paths. Most of the events used are too small for source mechanism solutions and thus we are not able to determine phase velocities using the single station method. Because of the size of events used (some as small as M4.3) and the limited response of the Kirnos sensors used at the former Soviet Union stations, we confine the period range of our study to between 30 and 70 seconds. Dispersion data in this range are sensitive to the crustal thickness and the S wave velocity in the uppermost part of mantle, but they cannot resolve well the velocity structures within the top part of the crust or in deeper part of the upper mantle.

In a previous paper by the senior authors on group velocity tomographic study (Wu and Levshin, 1994; hereafter called paper I), both Rayleigh and Love group velocity maps for China were obtained. Although the area studied in Paper I is contained in the present area, the inclusion of new Rayleigh data recorded in Tibet and recent data at the CDSN and SRO stations greatly enhanced the path density. As a result, the resolution of the velocity maps for some areas has improved, and some of the features are changed somewhat. In this paper we shall emphasize the new tomographic results in northern Asia, but we will describe the results for other areas for the sake of completeness. For more details on velocity maps of China and vicinity and on methodology, the reader should refer to Paper I. For this paper, in addition to the tomographic maps, inversion of average group dispersion curves sampled at twelve locations from the images was performed to obtain the S wave velocity structures. There structures provide a sample of the variations in crust and upper mantle.

The study area varies greatly in terms of basement geology and tectonic history. Fig. 1 shows the main tectonic units in this area as well as the general topography. The naming of the tectonic units are different in literature; for simplicity we shall follow that of the Sengor et al. (1993) for the major units

in northern Eurasia. It is commonly agreed that the Asian continent grew as a result of accretion of smaller continental fragments (Zonenshain et al, 1990; Coleman, 1989). The geologically ancient Angara craton can be viewed as the core, around which the Altaids, a wide belt of Paleozoic subduction-accretion complex (Sengor et al., 1993) developed. The Altaids is bordered on the south by a Paleozoic to Mesozoic collision suture that has since become an active orogenic zone sometime during the Cenozoic: this zone includes the following mountains: Tienshan in Kyrgyzstan and western China, to the north of Tarim basin, Beishan near the Mongolian border and Yinshan in northeastern China. The North China-Korean platform, composed of a series of Pre-Cambrian blocks, the Tarim, the Alan Shan, the Ordos and North China Plain (Fig. 1), are underlain by PreCambrian basement; these blocks are separated by presently active structures, and the North China Plain itself is undergoing extensional tectonics (Nabelek et al., 1987). South of this platform is the Paleozoic-Mesozoic suture along the Kunlun and the Astin Tagh mountain chain (north of the Tibetan plateau), the Nanshan (north of the Qaidam basin) and Qinling of eastern China. This is the suture along which Tibet and the South China block are attached to the rest of the continent. Except Qinling, the other parts of the suture has been reactivated. The western Tienshan is a very active tectonic zone, but eastern Tienshan, a belt of basins and ranges, is not so active (Figs. 1 and 2). The south China block was evidently attached to the rest of Asia in Permian, and it is one of the least active areas in China, except at its eastern edge, especially near Taiwan. It is underlain by Proterozoic to Mesozoic basement. The southern Tibetan block was accreted to northern Tibet in early Mesozoic and the impingement of the Indian plate along the Himalayan front that started about fifty million years ago had led to the formation of Tibet and the ongoing continental tectonics of the whole East Asian area (Molnar and Tapponnier, 1978). As shown in Fig. 1, many tectonic units are associated with distinct topographical expressions; thus the Angara craton, the West Siberian platform, the Tarim basin are all easily distinguished.

Fig. 2 shows the seismicity (1977-1992 and $M > 4.5$) of this area. By comparing the seismicity in the continental area and the topography as shown in Fig. 1, a close relationship between them can be seen; the seismicity has a tendency to attenuate gradually from the Tibet-India border toward the north and northwest (Fig. 2) and there is a corresponding descent from the top on the Pamir-Tibet plateau to the plains and hills of Siberia and eastern China (Fig. 1). There are a few conspicuous seismically quiet areas; the Tarim basin, the Ordos, the Ala Shan, the South China block, etc. Except for the South China block, these are identified as relatively rigid blocks that remain nearly undeformed among intensely deformed regions; they are underlain by PreCambrian basement as described above. The South China block lies in the stress shadow zone and is not seismic in general.

Since the study area includes some of the oldest cratons in Siberia, at a distance away from active zones, and PreCambrian terranes of substantial lateral extent amid active tectonic zones, it is interesting to see the corresponding variations of crustal and upper mantle structures under these areas. Elsewhere in the world, it is common to find that old shields are underlain by high velocity lid (Dorman and Ewing, 1962 ; Knopoff, 1983; Calcagnile and Scarpa, 1985; Snieder, 1988). Those areas however have not been subjected to recent tectonic activities. The overprint of younger tectonics on geologically ancient terranes presents an interesting problem in the study of crust and mantle structures. When rejuvenated tectonic activities are taking place, the deeper part of the crust and upper mantle under these terranes may be sufficiently modified by mantle processes and not be recognizable as such.

For Eurasia as a whole and using natural earthquakes as sources, Patton (1980) and Feng and Teng (1983) obtained the velocity structures of various portions by determining the Rayleigh wave dispersion curves for various parts of the area; while Patton (1980) defined the sub-regions based on topography and known crustal thickness, Feng and Teng (1983) divided the region into $10^o x 10^o$ grids; the paths used are relatively sparse in these studies because of the scarcity of data at the time and the resolution is rather coarse because of the grid size. For Siberia, a number of deep seismic profiles were made using artificial sources, and thus the crustal and mantle structures in that area are well delineated along those profiles. Egorkin et al. (1987) and Mechie et al. (1993) summarized the results along a number of profiles in the area of interest. We shall refer to these works in our discussion. Kozhevnikov and Barmin (1989) analyzed about 200 records of analog Soviet stations and several SRO stations deployed in Asia to obtain average Rayleigh wave group velocity curves for several pre-determined tectonic regions of Eastern Asia. These curves were used by Kozhevnikov et al. (1992) to find average lithosphere shear velocity structure for Tibet, the mountain region of Southern Siberia and Mongolia, platforms of South-eastern China and some other regions. With respect to Tibet, because of its unique tectonic characteristics, a number of studies were conducted. Chun and Yoshii (1977) used events on the eastern side of the Tibetan plateau and stations south of the Himalayas; they employed "regionalization" to obtain average crustal structure of the plateau. Brandon and Romanowicz (1986) employ the "two-event" technique to determine dispersion curves in northern Tibet. Bourjot and Romanowicz (1992) recently presented tomographic images of the Tibetan Plateau and its vicinity; they used two stations internal to China and several SRO stations in Asia and also ANTO in Turkey, GRFO in Germany and SSB in France. For eastern part of China, Weir (1983) determined group velocities along several paths using three SRO stations.

In this paper, we shall first present the Rayleigh group velocity images obtained through tomographic inversion. In order to learn about the velocity structures of some key areas, we invert the averaged dispersion curves obtained from these images. The images shear velocity models are then discussed in terms of their tectonic significance. We are particularly interested in the variation of crustal and upper mantle structures as a function of the age of the basement rocks and the intensity of recent tectonic activity.

Data

The data used for this study is a rather heterogeneous set, including Rayleigh dispersion data derived from three main sources: seismograms from M>6 earthquakes in Eurasia recorded at the Kirnos stations in the former Soviet Union collected by one of us (VMK), seismograms recorded at the SRO, CDSN and GSN stations in this region (obtained from IRIS/DMC), and and finally data from a temporary network of 11 stations established in Tibet from July 1991 to June 1992 (Owens et al., 1993). Fig. 1 shows the locations of these stations. The inclusion of data from stations established by the former Soviet Union in Mongolia and Siberia is important as data from these areas are were still somewhat lacking. Altogether 261 paths from these stations were available. Because of the wide dynamic range for the CDSN, the upgraded SRO seismic systems, and the portable broad band stations on the Tibetan plateau, the records stay on scale for $M_S > 6.5$ earthquakes, and, in some cases, surface waves from $M_S \tilde{} 4.3$ teleseismic events are recorded with good signal to noise ratio. Because most of the

events used are smaller than $M_S < 6$) and also the limited response of the Kirnos instruments, group velocities determination is limited in the 30-70 seconds range. For the CDSN/SRO dataset, 150 events, occurred in 1987, 1989, 1990, 1991 and the first half of 1992, were employed; the time spans used are related to the availability of data when they were acquired. With the temporary Tibetan array, we had, for the first time, extensive data internal to Tibet. Data from 30 events recorded at the array were used. All the events chosen for this study are located in and on the periphery of the area of interest. All in all, about 1200 event-station paths were finally chosen for the period range of 30-60 seconds; for 70 seconds only about half as many paths were used (Table I). The group velocity dispersion curves were determined with an interactive multiple filter group velocity program on a workstation, allowing rapid group velocity determination and visual quality control. Dispersion data are discarded when the sonogram shows complex envelop structures along the group arrival. In such cases we note that the waveform is usually more complex and relatively small, most probably radiated near the minimum of the radiation pattern and multipathing effects become pronounced.

Tomographic Methodology

To invert surface wave group velocities we applied a technique developed by Ditmar and Yanovskaya (1987) and Yanovskaya and Ditmar (1990). This technique can be considered a generalization of the Backus-Gilbert inversion method (Backus and Gilbert, 1968, 1970) for 2D problems. Input data for inversion are group travel times t_j for several fixed values T_m, $m = 1,...,M$, of period T along given paths L_i, $j = 1,...,J$, and corresponding cross-correlation matrices of travel time errors $R_t|_{T=T_m}$. Results of inversion are maps of group velocity distribution $U(\theta,\phi)|_{T=T_m}$ and a map of space resolution $R(\theta,\phi)$ for a given set of paths. Here θ and ϕ are latitude and longitude, respectively. The inversion procedure will be repeated for each period of interest. Much of the relevant theory behind the tomographic methodology is presented in paper I.

The 1D inversion

To invert for a one-dimensional structure at the particular geographical point we applied the following technique:

1. Extracting the one-dimensional group velocity curve from a set of tomographic maps for different periods.

The value of the group velocity for given period T was extracted from the corresponding group velocity map. Let us select the point with coordinates $\mathbf{r}_0=(\lambda,\phi)$. To avoid sharp kinks of the group velocities we applied a smoothing procedure:

$$\tilde{U}(T,\mathbf{r}_0)=\frac{\int_S U(T,\mathbf{r})W(\mathbf{r}-\mathbf{r}_0)d\mathbf{r}}{\int_S W(\mathbf{r}-\mathbf{r}_0)d\mathbf{r}}$$

where W is a Gaussian weight $W=\exp(-\alpha(\mathbf{r}-\mathbf{r}_0)^2)$, and the value of α was taken to be 0.5.

2. Inversion of group velocity curve for the one-dimensional structure at given geographical point $\mathbf{r}_0$.

We used with some modifications an algorithm developed by Lokshtanov (Kushnir et al., 1989). This algorithm combines the conjugate gradient scheme with randomized choice of a starting model.

The model is a flat-layered Earth with a fixed number of layers and free parameters. We used the 5-layered model with 3 crustal layers and two upper mantle layers including a halfspace for our final models. All shear velocities and all thicknesses of layers were considered as unknown; the half-space S-velocity is fixed and the P-velocities were related to S-velocities by Poisson ratio, and densities were fixed.

To make a 3D inversion we applied the technique described above for 1D inversion to points of a regular grid covering region under study. We used 2.6 degree increment in latitude and 5.2 degree increment in longitude. The same parametrization of the model was used for each point. Bi-spline interpolation between points was used to obtain maps of different parameters like layers' thicknesses or shear velocity values at different depths.

Tomographic images and S-velocity inversion results

The path coverage we are able to obtain with our present dataset and the spatial resolution map for Rayleigh waves at 40 seconds are shown in Fig. 3a and b, respectively; they are representative of the path coverage and resolution for 30-60 seconds data. The total number of paths used for each tomographic inversion, the corresponding initial group velocities and the mean square residuals for resulting models are presented in Table I. At 70 seconds, the coverage is much less dense, because of the limited energy for that period generated by the smaller events. Figs. 4a-e show the tomographic results for Rayleigh waves at 30, 40, 50, 60, and 70 second periods. To maximize the color scale contrast for these plots, we have chosen to set the minimum group velocity of each figure to red and the maximum to purple in the rainbow color scale. Note that the areas covered by the topographic map (Fig. 1) and the tomographic images and the resolution maps are the same.

It is important, when viewing the images, to know the resolution lengths of our tomographic results. As shown in Fig. 3b, the length is on the order of 300-500 km in much of Tibet, where our path coverage is very dense; it deteriorates sharply near the edge of the study area, where the path coverage is very poor (Figs. 3a and b). Features smaller than the resolution length for a particular area tend to be smeared. We also note that since these are group velocity images, the velocity structure at any point can be assessed after a dispersion curve is constructed from images for a range of periods and inverted. In the inversion, two approaches were taken. We first use a five layer structure with the bottom layer velocity fixed; the crustal velocities, the Moho depth and the upper mantle velocities are obtained through inversion. For region in which either the crustal thickness or the upper mantle velocities are at variance with structures determined through DSS profiling, then we adopt a three layer model, with the Moho depth fixed and invert for the crustal and upper mantle velocities. The dispersion curves constructed according to the method described earlier are shown in Fig. 5 and the results of the inversions are shown in Figs. 6 and 7. In this paper, all tomographic results were obtained assuming an isotropic model of the territory under study, pervious experiment with anisotropy modeling did not yield significant result (see Paper I).

The velocity maps (Figs. 4a-e) show that, in general, the Rayleigh group velocities are high in the northern part of the area, in Siberia, and the Tibet plateau is the center of a low velocity closure. There are many details in these maps that can be discussed in terms of tectonics. To facilitate our description

of the maps and the velocity models, we shall divide this area into seven sub-regions. More attention shall be given to well-resolved (with length = 1000*km*) areas not discussed in paper I and areas where images are noticeably enhanced over those of Paper I; those areas well resolved in Paper I will be reviewed for the sake of completeness. As can be seen in Figs. 1 and 3b, the Urals are on the edge of better resolved area and the East European platform, in the northwestern corner of our maps, is not well resolved at all and thus we will not discuss it here. We will only discuss areas with resolution length of roughly 1000 km or better. The geology is based mainly on Zonenshain et al. (1990) and Sengor et al. (1993).

1. Angara Craton

The Angara craton (Fig. 1) is also called Siberian platform (Zonenshain et al., 1990 and Egorkin et al., 1987). The craton is by no means uniform based on surface evidence. Rocks in the shield areas have isotopic ages as old as 3300-3650 Ma, and as a whole it probably became a continental landmass about 1700 Ma. Significantly, in various parts of the craton, there were extensive episodes of intraplate magmatism in Paleozoic and Mesozoic, flood basalt extrusion (255-245Ma) and kimberlite emplacement in Late Paleozoic and Mesozoic. Velocity models obtained along DSS profiles in this area (Yegorkin and Pavlenkova, 1981; Egorkin et al., 1987) show that it is underlain by crustal thickness varying from about 45 km in the central part of the craton to about 35 in the Vilyui depression in the southeast (Egorkin et al., 1987).

The tomographic images reveal this area to be one of relatively high group velocity for the period range of 40-70 seconds. It forms the contiguous northern Asia high velocity area. The sampled group velocity curve shown in Fig. 5 ("65.110"), together with that of the western Siberian platform ("60.80"), are the highest in the whole region. The unconstrained inversion results (Figs. 6, and Table I) show an average Moho depth of 28 km. The Moho shear velocity is about 4.6 km/s (Fig. 6). With the Moho depth constrained to 35 km, using results of Egorkin et al. (1987), we obtain an average mid-crustal S velocity of 3.72 km/sec and an upper mantle velocity of 4.54.

2. Western Siberian Platform

The platform is situated to the west of the Angara craton and east of the Urals (Fig. 1) and it is bordered on the south by the Tienshan. It is noted that while the northern part of this area is topographically flat area, the southern part rises gradually toward the south (Fig. 1). Sengor et al. (1993) deem it to be a part of the Altaids, formed in the Paleozoic as a result of progressive convergence between the Angara craton and North China (Zonenshain et al., 1990). It includes fragments of ancient massifs (1800 Ma-1900 Ma), oceanic complexes (1200-600 Ma), arcs, etc., and they were aggregated as a landmass in late Paleozoic. There is evidence for Mesozoic reactivation. In terms of recent tectonics, the northern part is not presently active as shown by its lack of topographic expression and seismicity (Figs. 1 and 2), but the southern part, near the northwestern border of China and the border of Mongolia, the seismicity becomes noticeable.

Although this area is geologically younger than the Angara craton and has a different tectonic origin, together with the craton, these two areas form the core of high velocity in Eurasia. In juxtaposition, the platform has even a slightly higher velocity than the cratonic mass, as can be seen especially in Figs. 4c and 4d. The sampled data in Fig. 5 ("60.80") are also seen to be slightly higher in values

than the data for Angara craton. In the unconstrained inversion for this area, the crustal velocities are slightly higher than those in the Angara area and the Moho depth deeper at 33 km. With Moho constrained at 35 km, the average crustal velocity is 3.73 km/sec, very similar to that under the Angara craton, and an upper mantle velocity of 4.6 km/sec.

3. Lake Baikal and Mongolia

Lake Baikal and Mongolia belong to two different tectonic provinces based on geological history. While Lake Baikal lies in a belt called Baykalides, a collision zone surrounding the Siberian platform that was formed somewhat earlier than the Altaids, Mongolia is within the Altaids (Fig. 1). It is well known that Lake Baikal is at the center of an active rift (Zorin et al., 1989).

While it is not surprising to see relatively high group velocity in the Lake Baikal area, as a result of thinned crust in a rift structure, it is not quite expected to find Lake Baikal at the head of a narrow high group velocity swath extending south-southwestward into central Mongolia. The flanking low in western Mongolia is more pronounced than that in the east. From Figs. 1 and 2, one can discern that western Mongolia is seismically more active and topographically more prominent than eastern Mongolia; this high group velocity ridge is essentially in the transition zone. In contrast to the Baikal area however, no prominent topographic depression exists, although there are smaller grabens in the northern part of the area marked by the high group velocity. We shall discuss this feature later in terms of known geology. Three points along the group velocity high were sampled: the middle section of Lake Baikal ("53.108"), northern central Mongolia ("48.103") and southern Central Mongolia ("45.100"). All these locations are along the group velocity low. The inversion for the central Lake Baikal site yields a crustal thickness of about 28 km, a relatively low velocity crust and upper mantle for the Lake Baikal site ("53.108" in Figs. 5 and 6; Table 2). At the other two sites ("48.103" and "45.100") along the low the crustal thicknesses are greater, but because of the narrowness of the high group velocity area, the group velocity curves may not have been properly sampled.

4. Northeast Siberian Fold System

The northeast Siberian folds are bordered on the west by the Verhoyansk mountains, a mountain chain formed of Late Paleozoic through Jurassic shallow water clastic sediments, representing the passive margin of the Siberian continent. Its main interior consists of exotic blocks and a series of Jurassic to Cretaceous igneous bodies. It is close to the present day continental margin and the circum-Pacific subduction system.

The resolution of the tomographic images (Fig. 3b) deteriorates in this area due to relatively sparse raypath coverage. At 70 seconds the northern part of the Verhoyansk mountains appear to be a relatively low velocity feature, but at all other periods, it is not distinguishable from eastern edge of the Angara craton. No velocity inversion was made for this region because of the low resolution of our results.

5. Tibet and Southwestern China

The Tibetan plateau is composed of blocks that were successively accreted during the Mesozoic and early Tertiary. The formation of the plateau probably occurred after mid- to late Miocene, and it is possible that major uplift occurred in Pliocene (Shackelton and Chang, 1988). Currently it is still a

very active structure with frequent large earthquakes in its interior and the seismic background is also fairly high (Fig. 2). It is clearly the most prominent topography in the whole region (Fig. 1).

The low group velocity feature associated with the Tibetan plateau and its surrounding area dominate all tomographic images (Figs. 4a-e). At 30 seconds the Rayleigh image (Fig. 5a) exhibits an extensive low velocity feature that covers the northern Tibetan plateau as well as a large portion of the western Tarim basin, the Pamirs, eastern Afghanistan northern Pakistan and western Yunnan, west of station KMI (Fig. 1) . The area of lowest velocity for Rayleigh waves is at its maximum for 40 seconds and it continues to shrink for longer periods, with central Tibet as the core of low group velocity at 70 seconds. With the shear wave velocities in the crustal and upper mantle column probably fairly similar across the plateau, the shape of the group velocity minimum at 70 seconds reflect the crustal thickness in Tibet. In most cases the low velocity closures extend to include parts of the Tarim and Qaidam basins.

Our tomographic images are quite comparable to those of Bourjot and Romanowicz's (1992). However, in their work the low velocity features are seen to persist up to 60 seconds, but as shown in Figs. 4a-e, we see it at 30-70 seconds, albeit the area is smaller at 70 seconds than at shorter periods. In southern Tibet, near the suture, the Rayleigh velocity increases sharply. Although the spatial resolution of the images starts to deteriorate there, the area is covered by a number of paths, and the relatively high velocity there is most probably correct.

The sampled group velocity curve for Tibet ("33.87" in Fig. 5) is very different from the other curves. The group velocity curve is essentially flat between 30 and 40 seconds. The unconstrained inversion results ("33.87" in Fig. 6) give a Moho depth of 60 km and a very low upper mantle S velocity of 4.23 km/s. The S velocities within the crust are also low. These results are reasonably consistent with with other results obtained by Wu et al. (1993), and no constrained inversion was made. The dispersion curves obtained in this study is quite different from those obtained using data from outside of Tibet and as a consequence the velocity structure is also different. We shall compare them later in the discussion section.

6. Tarim Basin and Tienshan

The Tarim basin is located in the southern part of the Altaids (Fig. 1); it is topographically quite distinct, as a relatively flat desert in among high mountains. Although the oldest rocks exposed in the basin (in western central Tarim along a thrust fault) is sedimentary rocks of Carboniferous age, it is assumed to be underlain by Archaen basement, based on outcrops on the rim of the basin (Ren et al., 1986). Remaining undeformed while neighboring Tibet and western Tienshan were subjected to enormous N-S strain, the Tarim has been interpreted to be a rigid block. The area is seismically less active than the surrounding areas as shown in Fig. 2. Gravitationally it appears as a well-defined area of relatively high Bouguer anomalies (Paper I). It is therefore somewhat surprising that Tarim, with its east-west dimension on the order of 1000 km and north-south width in excess of 500 km, does not have a corresponding expression in the tomographic images, especially in view of the fact that the spatial resolution there is on the order of 500 km. In fact as we pointed out above, southwest and western Tarim is a region of relatively low group velocity and forms a part of the Tibet low group velocity anomaly for Rayleigh waves at 30, 40, 50 and 60 seconds (Figs. 4). In Bourjot and Romanowicz' (1992)

tomography, similar results were obtained.

The Tarim basin is in a region of group velocity gradient; we did not attempt to construct an average group velocity curve. A group velocity curve is constructed in the western Tienshan area ("41.70" in Fig. 5) and the unconstrained inversion of this curve yield a Moho of 41 km and an upper mantle lid velocity of 4.2 km/s. When the Moho is constrained at 45 km, we obtain a average crustal velocity of 3.62 and an upper mantle velocity of 4.39 km/sec. These results are consistent with those of Yegorkin and Palenkova (1981) considering that the structure determined here is an average one.

7. Eastern China

The North China platform (includes areas marked #1 and #2, as well as North Korea, in Fig. 1) is composed of several blocks with different geological history and intensity of recent tectonics. The oldest rocks dated have isotopic ages of 3120 Ma (Yang et al., 1986). The North China Plain is underlain by a series of Neogene grabens developed in Proterozoic and perhaps older basement; the older rock are found on the edge of the basin. West of this Plain, the mountain front rises fairly steeply to a series plateaus underlain by Archaen rocks. While the North China Plain is known to be active, mainly as an extensional basin under NNW tension (Nabelek, 1987), the older blocks to the west, such as the Ordos platform, remain inactive (cf. Figs. 1 and 2). These blocks are, however, separated by active structures such as the Shenxi graben east of the Ordos platform.

The South China platform is separated from the North China platform by the Qinling mountains (Fig. 1); the northern edge of the Qinling is probably the suture along which the two parts of eastern China were hinged together in Permian (Yang et al., 1986). The basement of the South China platform is Proterozoic. In so far as young tectonics and seismicity are concerned, the South China platform as a whole is the least active part of eastern Asia. Some seismicity is present in the southeast coastal China, near Taiwan, probably related to the collision tectonics there.

In the group velocity maps, especially in Figs. 4b-d, a high group velocity gradient in eastern China is seen to extend from just east of Mongolia to south China. This gradient is nearly coincident with the gradient in the topography (Fig. 1) and in Bouguer gravity (paper I). This zone is traditionally taken as the transition across which the Moho depth changes rapidly (Wang and Mao, 1985). Reflection and refraction profiles in this area (Wang and Mao, 1985) show that the crust is relatively thin with the Moho at about 32 km; it is a sharp decrease from the 40 km thick crust west of the transition. In our tomographic images, the North China Plain (Fig. 1) emerges as a region with relatively high group velocity at 40 seconds (Figs. 4b) and the region broadens westward at 50 and 60 seconds to include Ordos platform (compare Figs. 1, 4b and 4c). The dispersion curve for the North China Plain area ("38.117" in Fig. 5), show that the group velocity rises sharply until 60 seconds, and beyond that period the curve flattens. Thus, at 70 seconds (Fig. 4e) the North China plain is no longer a noticeable high velocity area. The unconstrained inversion result (Fig. 6, "38.117") shows a relatively thin crust of 27 km, and an uppermost mantle S velocity of 4.4 km/s. No constrained inversion was performed as this result is consistent with that of Weir (1982).

Much of the South China platform is a relatively high group velocity region at 40-60 seconds for Rayleigh waves (Figs. 4b-d). A low velocity ridge, starting from southern Ryukyu and continue northwestward along a portion of the southern boundary of the North China-Korean platform, seems to

exist at all periods studied (Figs 4a-e). This is an interesting feature that cannot easily be explained on the basis of surface geology or Bouguer gravity (Paper I). The group velocity curve is shown in Fig. 5 ("24.110") and the inversion results in Fig. 5 shows a thin crust of 26 km and an uppermost mantle S velocity of 4.33 km/s.

8. 3-D Inversion result

Fig. 7 shows the S-wave velocity distribution at 60 km, resulting from a 3-D inversion of the tomographic maps (Figs. 4a-e). Because the inversion is done on a fairly coarse grid (see Methodology), the velocity map obtained is highly smoothed. For most of the areas on this map, Fig. 7 shows the velocity in the upper mantle, but in Tibet, the S-wave velocity near the bottom of the crust is shown. At the other depth, the current results are too noisy for further study.

Discussion

Tomographic inversion of a densely distributed group dispersion dataset in eastern Eurasia yields well resolved group velocity images for much of the area. The resolution of the maps are not uniform, being better in the China, where the gathering of modern digital data started earlier than in other parts. The addition of data at the stations equipped with Kirnos seismometers in the former Soviet Union was important for resolving better the details in Siberia. With the current resolution of about 350-1000 km, we can correlate the images with many of the major geological features in Eurasia. In contrast to global tomographic studies (Zhang and Tanimoto, 1993), in which the resolution length is on the order of 1000 km, the images presented in this paper have enough details to compare to the large scale geologic structures observed on the surface. Besides defining the structural units in terms of group velocity, the images also reveal some features that are not shown in surface geology. Through constrained or unconstrained inversion of the group velocity dispersion curves derived from the tomographic images, we are able to determine S wave velocity structures or the thicknesses of the crust in various key locations.

Within Eurasia, the tectonic history varies greatly from region to region. The Rayleigh group velocity tomographic images shown in Figs. 4a-e provide a synoptic view of the variations in terms of group velocity. With the period ranging from 30 to 70 seconds, the maps indicate the variations of velocity structures in the lower crust and uppermost part of the mantle.

That the Angara craton is underlain by high velocity crust and uppermost mantle is consistent with observations in PreCambrian terranes in Scandinavia and elsewhere (Snieder, 1988 and Calcagnile et al., 1985). The Angara craton, together with the Western Siberian platform, a Paleozoic collision complex, form the high velocity core of Asia. The western Siberian platform has thinner crust, and therefore appears as a high group velocity area in the group velocity image (Figs. 4). We note that the Angara craton underwent significant extension in the Paleozoic and Mesozoic and has an higher average elevation (Fig. 1), resulting in a thicker crust. The younger western Siberian platform has not had significant tectonic modification since its formation (Zonenshain et al., 1990). The nearly total absence of seismicity (Fig. 2) indicates that the post-Tertiary reactivation of Eurasia as a result of impingement of the Indian subcontinent has not affected this area. The structure determined from our dispersion curve for the western Siberian platform is quite similar to that of Egorkin et al. (1987). For the Angara platform, we have constrained the Moho depth and the average crustal S wave velocity in that case

agree with those of Egorkin et al. (1987), assume a $\frac{V_p}{V_s}$ of 1.80.

There are many other geologically ancient terrains in this area as we have described earlier. They include the Ordos, Shanxi, the Alashan, the Sichuan basin, the North China Plain, etc. Unlike the Siberia shields, however, they do not show up as distinct high group velocity features. The size of these blocks are not as large as Siberia, but if the Lake Baikal rift as well as several other smaller units can be resolved as well as we have, then these features should be resolvable as well. While Ordos is noticeably aseismic and lacking other signs of recent tectonic activities, other terrains are either currently active, as are Shanxi, Alashan and the North China Plain.

The Baikal rift south of the Siberian platform is well-known as an active feature (Zonenshain, 1990); the rift valley is a remarkable topographic feature and the area is seismically quite active (Fig. 2). The lithosphere in the rift valley area is found to be quite thin, about 40-50 km, and the crust is estimated to be less than 35 km, based on gravity and limited seismic data (Zorin et al., 1993). The high velocity ridge in the tomographic group velocity images as well as the 60 km S-wave velocity map (Figs. 4 and 7) are consistent with these results, although the group velocity inversion results give a much shallower Moho. Lacking constraints at the shorter period range could have biased our results toward lower velocities in the crust and therefore shallower Moho.

The continuation of the Baikal rift high velocity into Mongolia was not suspected initially. Although little geophysical data are available in this area, Russian and Mongolian geologists have postulated that the area in Mongolia where the high velocity ridge is seen, is underlain by an upper mantle structure similar to that under the Baikal rift (see Windley and Allen, 1993, for a review). South of Lake Baikal, there are several north-south striking rifts, the Hobsogol, Oka, etc., but further south, down to 46° S, there are only a few short and narrow ones mapped. However, the area of high velocity nearly coincides with the area of late Cenozoic basaltic (Windley and Allen, 1993). Our data shows that it is quite possible that an "asthenosphere bulge" exists in this area. The Lake Baikal and the central Mongolian structures combine to form one of the major active tectonic element within the Eurasian continent.

The low velocity extreme in this area is exhibited by the Tibetan plateau. It represents the most prominent topography on the Earth and its subsurface structures have been under intense investigation (Hirn et al., 1988; Beghoul, Barazangi and Isacks, 1993; Zhao et al., 1994). Most of the studies so far are limited by geographic access to this vast area. In that it is extremely difficult to deploy stations in the Tibetan interior, tomographic studies will probably provide the best chance to resolve the question of the lateral variations of structures within the plateau. Our results already show that southern Tibet, near the Zangbo suture and the Himalayas, is a region of relatively high velocities, in comparison to the rest of the plateau. This result agrees with that of Jobert et al. (1985) obtained with instruments inside Tibet. As far as the interior of the plateau is concerned, it appears that the plateau has a bowl shaped Moho with its bottom in central Tibet. Its extension westward toward the Pamirs is quite clearly expressed in the images. The unconstrained velocity inversion for the Tibetan plateau yields an average Moho depth of 60 km Table 1). It has very low crustal velocity and low upper mantle velocity.

The extension of the Tibetan low velocity under southern Tarim, supposed to be a fairly rigid Pre-Cambrian block, is quite clearly shown in 4a-d. Tarim is not very active, seismically speaking, but the western part is known to have an E-W oriented active thrust fault (e.g., Ren et al., 1987). Thus, although it might be a region with geologically ancient basement, it is a currently active area. Judging from the fact that we can resolve more rapidly varying features such as the transition from central to southern Tibet, the gradual nature of this transition from Tibet to Tarim is real. It is also observed by Bourjot and Romanowicz (1992). It appears that tectonic activities under Tibet is spreading to the neighboring areas to the north.

Ideally we should invert for velocity directly through a two step process as is done by The velocity structures obtained in this study are In that it is extremely difficult to deploy stations in the Tibetan interior, tomographic study will probably provide the best chance to resolve the question of the lateral variations of structures within the plateau. Southern Tibet, near the Zangbo suture and the Himalayas, is a region of relatively high velocities, in comparison to the rest of the plateau. This result agrees with that of Jobert et al. (1985) obtained with instruments inside Tibet. It is interesting that the Tibetan low velocity seems to extend under southern Tarim, supposed to be a fairly rigid Pre-Cambrian block. Tarim is not very active, seismically speaking, but the western part is known to have an E-W oriented active thrust fault in the middle part of the basin (Ren et al., 1987). Thus, although it might be a region with geologically ancient basement, it is a currently active area.

We have noted earlier that the Tienshan fold belt as east of longitude $87^{\circ}E$ (Fig. 1) is noticeably distinct from the western part in that whereas the western part reveals itself as an area with low Rayleigh wave group velocity, the eastern part is an area of relatively high velocity. This feature seems to be consistent with the observation that the Bouguer gravity low (Fig. 2) associated with western Tienshan (the -250 mgal contour) terminates there. Also, as noted earlier, the Tienshan here is actually a E-W striking basin and range province, with the presence of the sub-sea level Turfan basin as the lowest point. Evidently, this is a deep-seated feature, with a thin crust underneath, resulting perhaps from north-south tension. The seismicity of western section of Tienshan is rather high with large thrust events; in contrast eastern Tienshan is not very seismic (Fig. 10).

The increase in group velocities of both the Rayleigh eastward across $105^{\circ}E$ is clear in Figs. 4. The trend agrees generally with that shown in the Bouguer gravity map (Paper I). In the eastern half of the study area, the relatively high velocity region south and east of Beijing (the North China Plain) is easily distinguished; it is evidently related to the thin crust in that region, with thickness generally less than 35 km (Wang and Mao, 1985). The North China Plain is a region of active extensional tectonics (Nabelek et. al., 1987) where many large earthquakes were located.

Southeastern China is also a region of relatively high velocities especially at periods less than 70 seconds. Here the thin Archaen crust (~32 km) is probably the main controlling factor. In contrast to North China Plain, this region is not tectonically active. The Japan Sea area appears as a high velocity region for Love and Rayleigh waves at 40 seconds (Figs. 6a and 8a), but becomes an area of relatively low velocity for longer period Rayleigh waves (e.g., Fig. 6d and 6e).

Conclusion

The Rayleigh group velocity imaged of a large part of Eurasia reveal many features that can readily be correlated with known surface geology and interesting features not previously known from surface mapping. In terms of previously unsuspected features, the group velocity high extending south from Lake Baikal to Mongolia is a good example. But the geologically and topographically distinct Tibetan plateau is seen as a large well defined area with extremely low group velocities. It is almost certain that we did not recover the full amplitude of the anomaly associated with Tibet, because we did not take into account of the bending of rays. In fact, strong focusing and defocusing must occur, depending on the exact location of receivers, for rays passing through Tibet.

As a result of the establishment of new high quality digital stations in Eurasia, we can study the continental structures under Eurasia in more detail. In that Eurasia is very large and some parts are very remote, tomography provides a method for uniformly sampling the region and for resolving lateral variations. By using group velocity dispersion data as datum for this paper, we are able to obtain relatively high path density. With continued accumulation of data at the Global Seismic Network stations, one should be able to use data from larger earthquakes, for which the CMT solutions are available, and achieve similar path density.

This

Acknowledgement

This study was supported by National Science Foundation grants EAR-9004220 and EAR-9206545 and the Air Force Phillips Laboratory contract F1962890K0042 and NSF grant EAR9004220. We are thankful to Drs. Tatyana Yanovskaya and Paul Ditmar from the University of St.-Petersburg, Russia for providing us with their tomographic inversion program. We thank Dr. Dmitri Lokshtanov from Norsk Hydro, Norway for providing us with his program for group velocities 1D-inversion. We would like to thank Y. L. Kung, Robin Martin, R. J. Rau, and D. Salzberg of SUNY Binghamton for assistance.

References

Backus, G. and Gilbert, F., 1968. The resolving power of gross Earth data. Geophys. J. Roy. Astr. Soc., 16: 169-205.

Backus, G. and Gilbert, F., 1970. Uniqueness in the inversion of inaccurate gross Earth data. Phil. Trans. Roy. Soc. London, 226: 123-192.

Baljinnyam, I., and 11 others, 1993. Ruptures of major earthquakes and active deformation in Mongolia and its surroundings, Geological Society of America Memoir 181, Boulder, Colorado, 62pp.

Beghoul, N., Barazangi, M., and Isacks, B.L., 1993. Lithospheric structure of Tibet and western North America: mechanism of uplift and comparative study, J. Geophys. Res., 98, 1997-2016.

Bourjot, L., and Romanowicz, B., 1992. Crust and upper mantle tomography in Tibet using surface waves. Geophys. Res. Lett., 19: 881-884.

Brandon, C., and Romanowicz, B., 1986. A "no-lid" zone in the central Chang-Thang platform of Tibet: Evidence from pure path phase velocity measurements of long period Rayleigh waves. J. Geophys. Res., 91: 6547-6564.

Brune, J.N., and Dorman, J., 1963. Seismic waves and Earth structure in the Canadian Shield. Bull. Seism. Soc. Am., 53: 167-509.

Calcagnile, G., and Scarpa, R., 1985. Deep structure of the European-Mediterranean area from seismological data. Tectonophysics, 118, 93-111.

Chun, K. Y., and McEvilly, T. V., Crustal structure in Tibet: High seismic velocity in the lower crust. J. Geophys. Res., 91, 10405-10411, 1986.

Chun, K. Y., and Yoshii, T., Crustal structure of the Tibetan Plateau: A surface wave study by a moving window analysis, Bull. Seismo. Soc. Am., 67, 737-750, 1977.

Coleman, R. G.,1989. Continental growth of Northwest China, Tectonics. 8, 621-635.

Ditmar, P.G., and Yanovskaya, T.B., 1987. A generalization of the Backus-Gilbert method for estimation of lateral variations of surface wave velocity. Izv. AN SSSR, Fizika Zemli (Solid Earth), no. 6: 30-60.

Dorman, J. and Ewing, M., 1962. Numerical inversion of seismic surface wave dispersion data and crust-mantle structure in the New York-Pennsylvania area. J. Geophys. Res., 67, 5227-5241.

Feng, C. C., and Teng, T., 1983. Three-dimensional crust and upper mantle structure of the Eurasian continent. J. Geophys. Res., 88: 2261-2272.

Feng, R., Zhu, J.S., Ding, Y.Y., Chen, G.Y., He, Z.Q., Yang, S.B., Zhou, H.N. and Sun, K.Z., 1983. Crustal structure in China from surface waves. Chinese Geophysics, Am. Geophys. Union, 2: 273-289.

Hirn, A., 1988. Features of the crust-mantle structure of Himalayas-Tibet: a comparison with seismic traverses of Alpine, Pyrenean and Variscan orogenic belts. Phil. Trans. Roy. Soc. London. A 327: 17-32.

Jobert, N. and Jobert, G., 1983. An application of the ray theory to the propagation of waves along a laterally heterogeneous spherical surface. Geophys. Res. Lett., 10: 1148-1151.

Jobert, N., Jounet, B., Jobert, G., Hirn, A., and Sun, K.Z., 1985. Deep structure of southern Tibet inferred from the dispersion of Raleigh waves through a long-period seismic network, Nature, 313, 386-388.

Knopoff, L., 1983. The thickness of the lithosphere from dispersion of surface waves, Geophys. J. Roy. Astro. Soc., 74, 55-81.

Kozhevnikov, V.M. and Barmin, M.P., 1989. Dispersion curves of Rayleigh wave group velocities for several regions of the Asian continent. Izv. AN SSSR, Fizika Zemli (Solid Earth), no. 9: 16-25.

Kozhevnikov, V.M., Lokshtanov, D.E. and Barmin, M.P., 1992. Shear-velocity structure of the lithosphere for nine large tectonic regions of the Asian continent. Izv. AN SSSR, Fizika Zemli (Solid Earth), no. 1: 61-70.

Kushnir, A.F., Levshin, A.L., Lokshtanov, D.E., 1989. Determination of the velocity cross-section from the spectra of surface waves by nonlinear optimization methods. In: "Problems of Seismological Information Science, Comput. Seismology", ISS. 21, Allerton Press, NY, 127-141.

Levshin, A.L., Yanovskaya, T.B., et al., 1989. Seismic Surface Waves in a Laterally Inhomogeneous Earth. Editor Keilis-Borok, V.I., Kluwer Acad. Publ., Dordrecht/ Boston/ London.

Mechie., J., Egorkin, A.V., Fuchs, K., Ryberg, T., Solodilov, L., Wenzel, F., 1993, P-wave mantle velocity structure beneath northern Eurasia from long-range recordings along the profile Quartz, Phys. Earth and Planet. Inter.: 79, 269-286.

Molnar, P., 1988, A review of geophysical constraints on the deep structure of the Tibetan Plateau, the Himalaya and the Karakoram and their tectonic implications. Phil. Trans. Roy. Soc. London. A 327: 33-88.

Molnar, P., And Lyon-Caen, H., 1989. Fault plane solutions of earthquakes and active tectonics of the Tibetan Plateau and its margins, Geophys. J. Int., 99: 123-153.

Molnar, P. and Tapponnier, P., Active tectonics of Tibet, J. Geophys. Res., 83: 5361-5375.

Nabelek, J., Chen, W.P., And Ye, H., 1987. The Tangshan earthquake sequence and its implications for the evolution of the North China Basin. J. Geophys. Res., 92: 12615-12628.

Owens, T.J., Randall, G.E., Wu, F.T. and R.S. Zeng, 1993. PASSCAL instrument performance during the Tibetan plateau passive seismic experiment, Bull. Seism. Soc. Am., 83, 1959-1970.

Patton, H., 1980. Crustal and upper mantle structure of the Eurasian continent from the phase velocity and Q of surface waves. J. Rev. Geophys. Space Phys. 18: 605-625.

Ren, J.S., Jiang C.F., Zhang, Z.K. and Qin, D.Y., 1986. Geotectonic Evolution of China. Springer-Verlag, New York, 203p.

Sengor, A.M.C., Natal'in, B.A., and Burtman, V.S., 1993. Evolution of the Altaid tectonic collage and Palaeozoic crustal growth in Eurasia. Nature: 364, 299-307.

Shackelton, R.M. and C.F. Chang, 1988. Cenozoic uplift and deformation of the Tibetan plateau: the geomorphic evidence. Phil. Trans. Roy. Soc. London. A 327: 365-377.

Snieder, R., 1988. Large-scale waveform inversions of surface waves for lateral heterogeneity, 2. Application to surface waves in Europe and the Mediterranean. J. Geophys. Res., 93, 12067-12080.

Terman, M., 1973. Tectonic Map of China and Mongolia. Geol. Soc. of Am., Boulder, Colorado.

Tikhonov, A.N. and Arsenin,V., 1976. Methodes de resolution de problemes mal poses. MIR Publishers, Moscow.

USAF, 1971. Bouguer gravity anomaly map of Asia. Aeronautical Chart and Information Center, St. Louis, Mo., USA.

Wang, G.Z., and Mao, E.T., (Eds.) 1985. Crust and Upper Mantle in China, Results of Geophysical Exploration. Seismological Press, Beijing, China.

Wier, S. 1982. Surface wave dispersion and Earth structure in South-Eastern China. Geophys. J. Roy. Astr. Soc., 69: 33-47.

Windley, B.F., Allen, M.B., 1993. Mongolian plateau: Evidence for a late Cenozoic mantle plume under central Asia, Geology, 21, 295-298.

Wu, F.T., and A. Levshin, 1994. Surface-wave group velocity tomography of East Asia, Phys. of Earth and Planet. Int., 84: 59-77.

Yang, Z.Y., Cheng, Y.Q., Wang, H.Z., 1986. The Geology of China. Clarenden Press, Oxford.

Yanovskaya, T.B., 1982. Distribution of surface wave group velocities in the North Atlantic. Izv. AN SSSR, Fizika Zemli (Solid Earth), no. 2: 3-11.

Yanovskaya, T.B. and Ditmar, P.G., 1990. Smoothness criteria in surface wave tomography. Geophys. J. Int., 102: 63-72.

Yegorkin, A.V. and Pavlenkova, N.I., 1981. Studies of mantle structures of U.S.S.R. territory on long-range seismic profiles, Phys. of Earth and Planet. Int., 25, 12-26.

Zhao, Wenjin, Nelson, K.D., and Project Team, 1994. Deep seismic reflection evidence for continental underthrusting beneath southern Tibet, Nature, 366, 557-559.

Zonenshain, L.P., Kuzmin, M.I., and Natapov.,L.M., 1990. Geology of the USSR: A plate-tectonic synthesis, Geodynamics ser. vol. 21, Am. Geophys. Union, Washington, D.C.

Zorin, Y.A., Kozhevnikov, V.M., Novoselova and Turutanov, E.K., 1989. Thickness of the lithosphere beneath the Baikal rift zone and adjacent regions, Tectonophysics, 168, 327-337.

Figures

Figure 1. Topography of Eastern Asia based on the ETOPO5 topographic database with generalized tectonics superposed (after Sengor et al., 1993 and Terman, 1973). The numbered features are (1) North China Plain, (2) The Ordos Platform, (3) the Ala Shan Block, (4) The Tarim Basin, [these four, together with North Korea, are often collectively called North China-Korean Platform], (5) Qaidam Basin, (6) Tibetan Plateau, (7) Sichuan Basin, (8) South China Platform, (9) Sung-Liau Plain and (10) Tienshan. The locations of seismic stations used in the study are shown as triangles. Station CHTO is below latitude 20 at longitude 100 E. The HIA, MDJ, BJI, LZH, WMQ and KMI are part of the Chinese Digital Seismographic Network (CDSN). The stations in the former Soviet Union and Mongolia, except ARU, KIV, GAR and AAK, which are now a part of the Global Seismic Network, are stations established by the former Soviet Union. Notice that many of the tectonic units shown in this figure are clearly associated with major topographical features. The Tibetan Plateau is the most prominent feature on this map. Some of lesser features can be seen in this map. For example, although the eastern section of Tienshan southeast of WMQ station is a continuation of the western Tienshan, it is actually a basin and range area with its lowest point in the Turfan Basin (-280m). The Szechuan Basin (#7, the bluish area north of KMI station) is surrounded by 1000-2000 mountain ranges. The general decrease in topography from Tibet to western China can be clearly seen. The diamonds mark the location where average dispersion curves are constructed and one dimensional velocity structures obtained.

Figure 2. Seismicity of the study area. Data include epicenters of all events of M>4 from 1977-1992 published by USGS in the Preliminary Determination of Epicenters (PDE). The epicenters are marked as circles.

Figure 3. (a) Path coverage for this study. Along most of the paths both Love and Rayleigh waves are available. For different periods the coverage varies slightly. (b) Resolution of tomographic inversion results for Rayleigh Waves at 50 seconds.

Figure 4. Rayleigh wave group velocity tomographic inversion results for (a) 30 seconds, (b) 40 seconds, (c) 50 seconds, (d) 60 seconds, and (e) 70 seconds. Note that a different velocity scale is used for each figure.

Figure 5. Group velocity data (points) obtained by taking an average value around the points marked by diamond in Fig. 1 and the synthetic curves calculated from inversion models. The numbers in each frame correspond to the latitude and longitude of the sampling point.

Figure 6. Velocity structures obtained at twelve locations shown in Fig. 1. The numbers in each frame correspond to the latitude and longitude of the sampling point.

Figure 7. S-wave velocity at 60 km depth, obtained by inverting the group velocity maps.

Figure 8. Map showing location of Cenozoic basaltic volcanism. Compare the region to the high group ridge in the topo tomographic images.

Table 1

Inversion parameter and residuals for different waves and periods

Period	Number of	Average velocity	Average residual
Sec	paths	km/s	Sec
30	1165	3.09	31.8
40	1158	3.30	32.0
50	1109	3.45	29.5
60	935	3.58	24.7
70	511	3.63	21.8

Table 2 Velocity Models

W. Siberian		Angara		E. Russia		Baikal	
depth	velocity	depth	velocity	depth	velocity	depth	velocity
0.	3.32	0.	3.10	0.	2.63	0.	2.69
5.	3.34	6.	3.09	5.	3.24	5.	3.24
22.	3.37	17.	3.18	17.	3.31	16.	3.49
33.	4.58	28.	4.58	28.	4.49	26.	4.44
83.	4.50	78.	4.50	79.	4.50	77.	4.50

Pamir		W. Mongol.		C. Mongol.		Japan Sea	
depth	velocity	depth	velocity	depth	velocity	depth	velocity
0.	3.28	0.	2.93	0.	2.87	0.	3.02
5.	3.42	5.	3.20	5.	3.41	4.	3.31
29.	3.43	18.	3.20	16.	3.44	16.	3.44
41.	4.20	29.	4.27	34.	4.39	26.	4.36
93.	4.50	80.	4.50	83.	4.50	77.	4.50

Tibet		S. Mongol.		N. China		S. China	
depth	velocity	depth	velocity	depth	velocity	depth	velocity
0.	2.74	0.	3.11	0.	2.81	0.	2.93
5.	3.38	4.	3.47	5.	3.09	5.	3.12
29.	3.37	24.	3.53	17.	3.40	16.	3.19
60.	4.23	40.	4.48	27.	4.40	26.	4.33
110.	4.50	91.	4.50	78.	4.50	78.	4.50

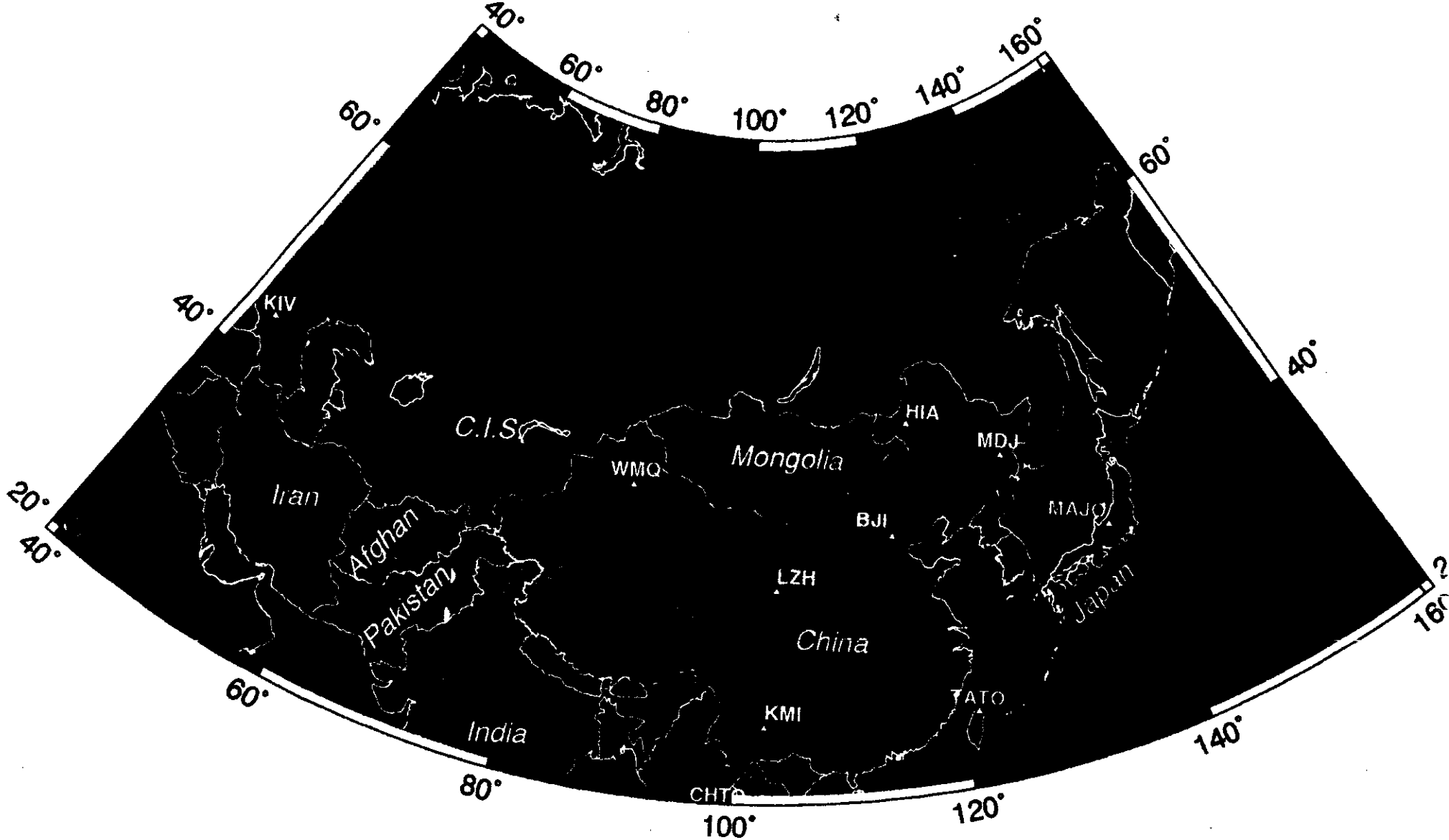
40°
60°
80°
100°
120°
140°
160°
60°
40°
20°
KIV
C.I.S.
HIA
MDJ
WMQ
Mongolia
Iran
Afghan
Pakistan
BJI
MAJO
LZH
China
Japan
India
KMI
TATO
CHT

Fig 1

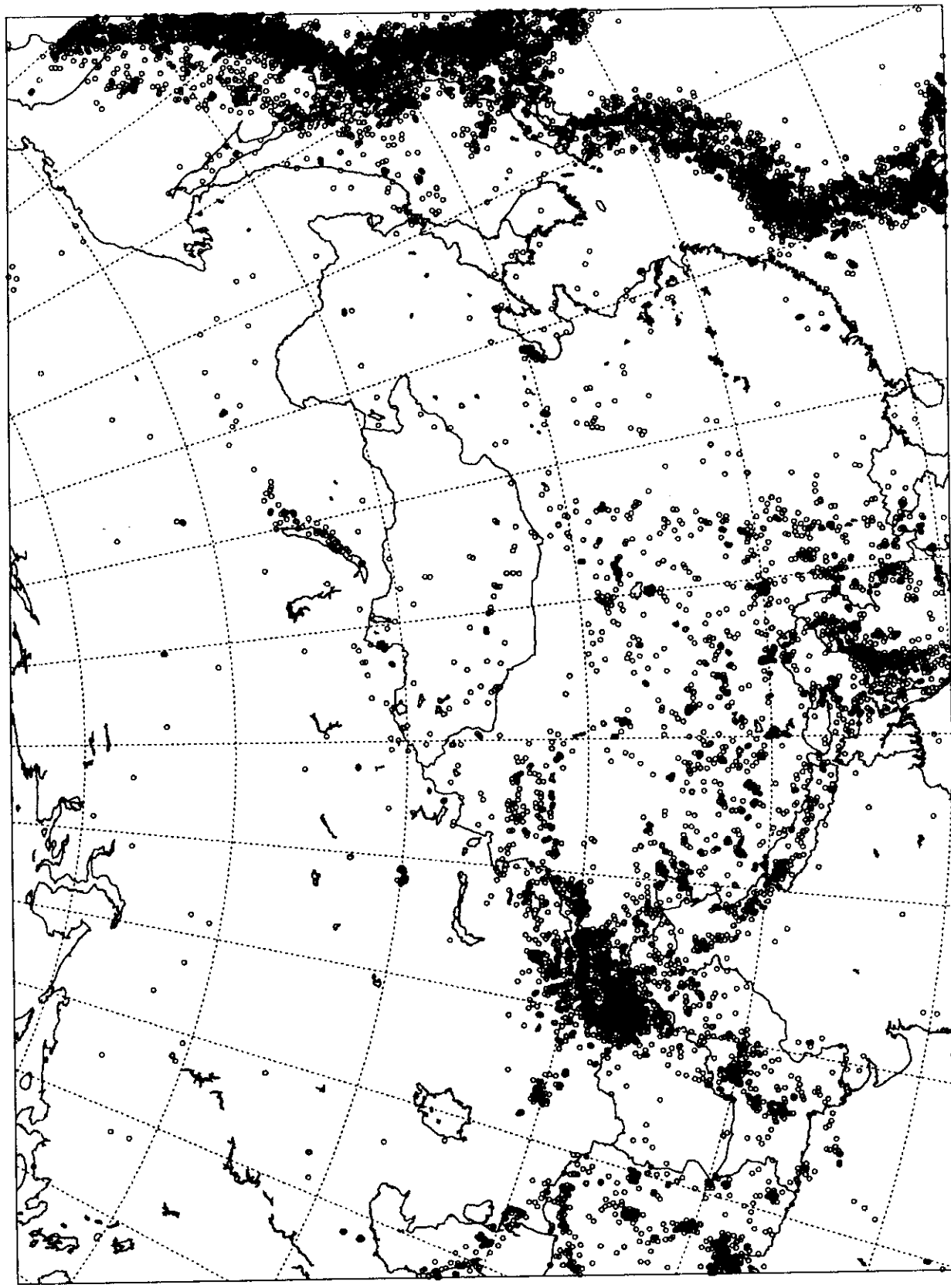

Fig 2

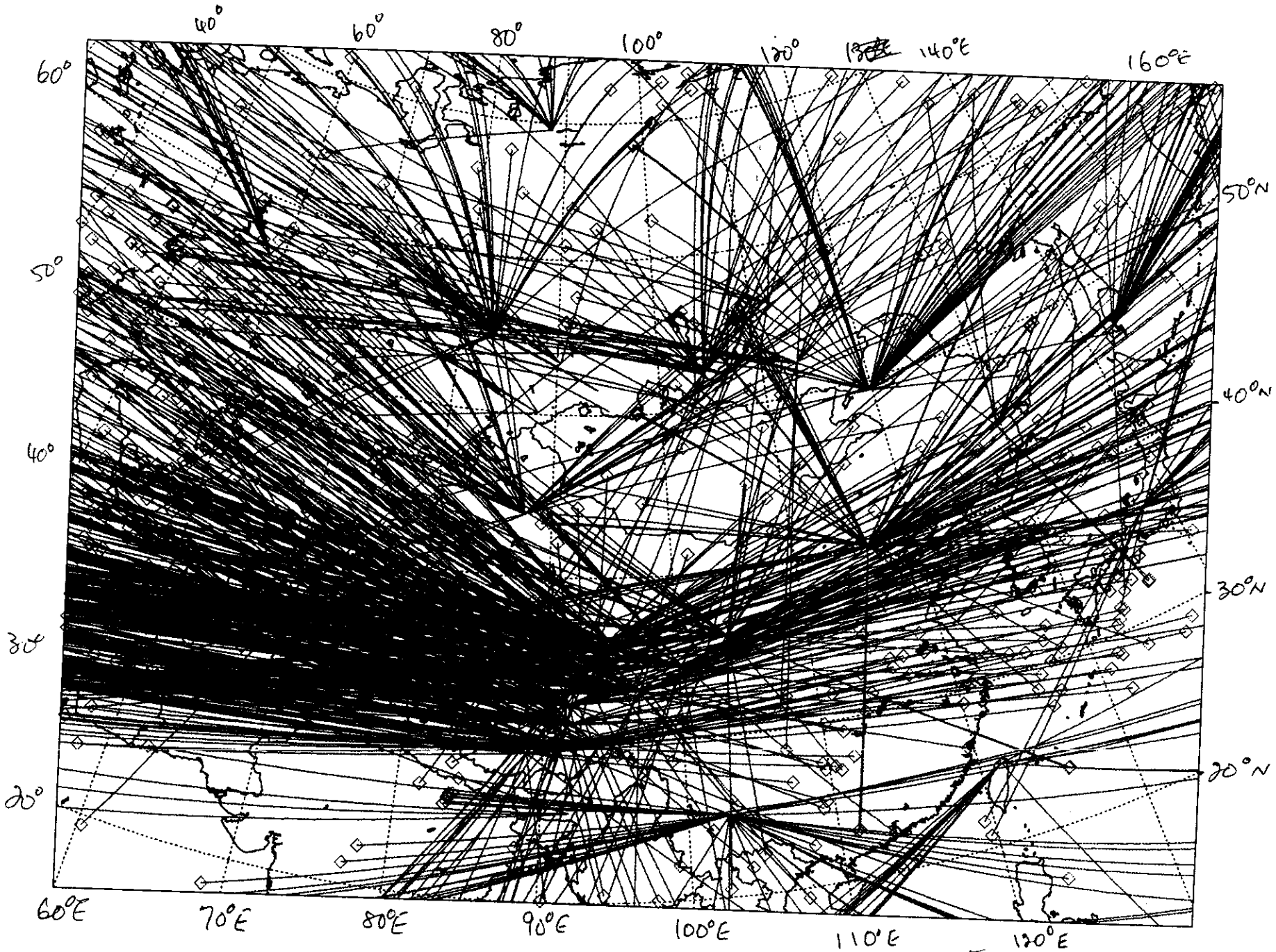
40°
60°
80°
100°
120°
140°E
160°E
60°
50°
40°
30°
20°
50°N
40°N
30°N
20°N
60°E
70°E
80°E
90°E
100°E
110°E
120°E

Fig 3a

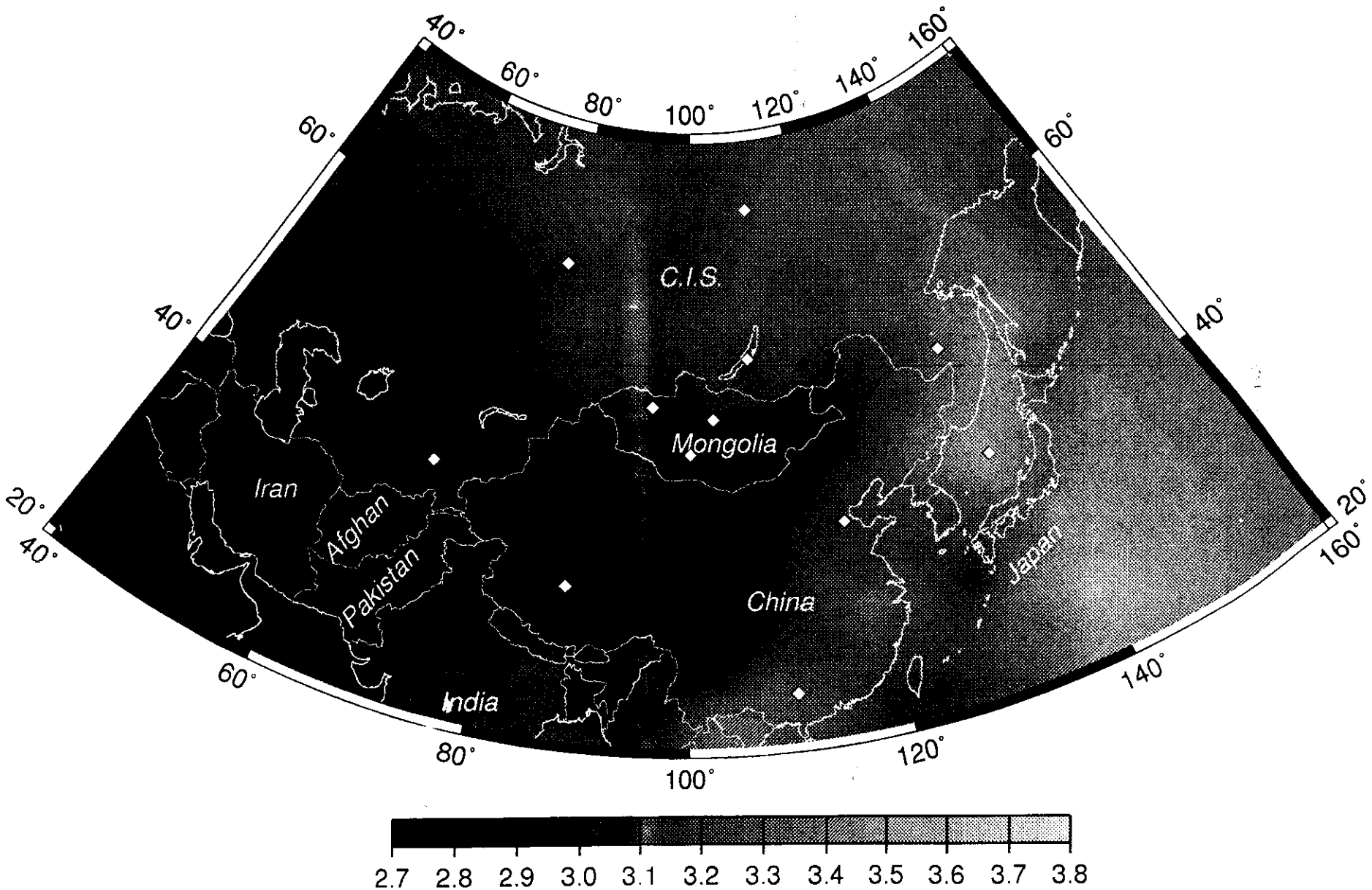
40°
60°
80°
100°
120°
140°
160°
60°
40°
20°
C.I.S.
Mongolia
Iran
Afghan
Pakistan
China
India
Japan
2.7
2.8
2.9
3.0
3.1
3.2
3.3
3.4
3.5
3.6
3.7
3.8

Fig 4a

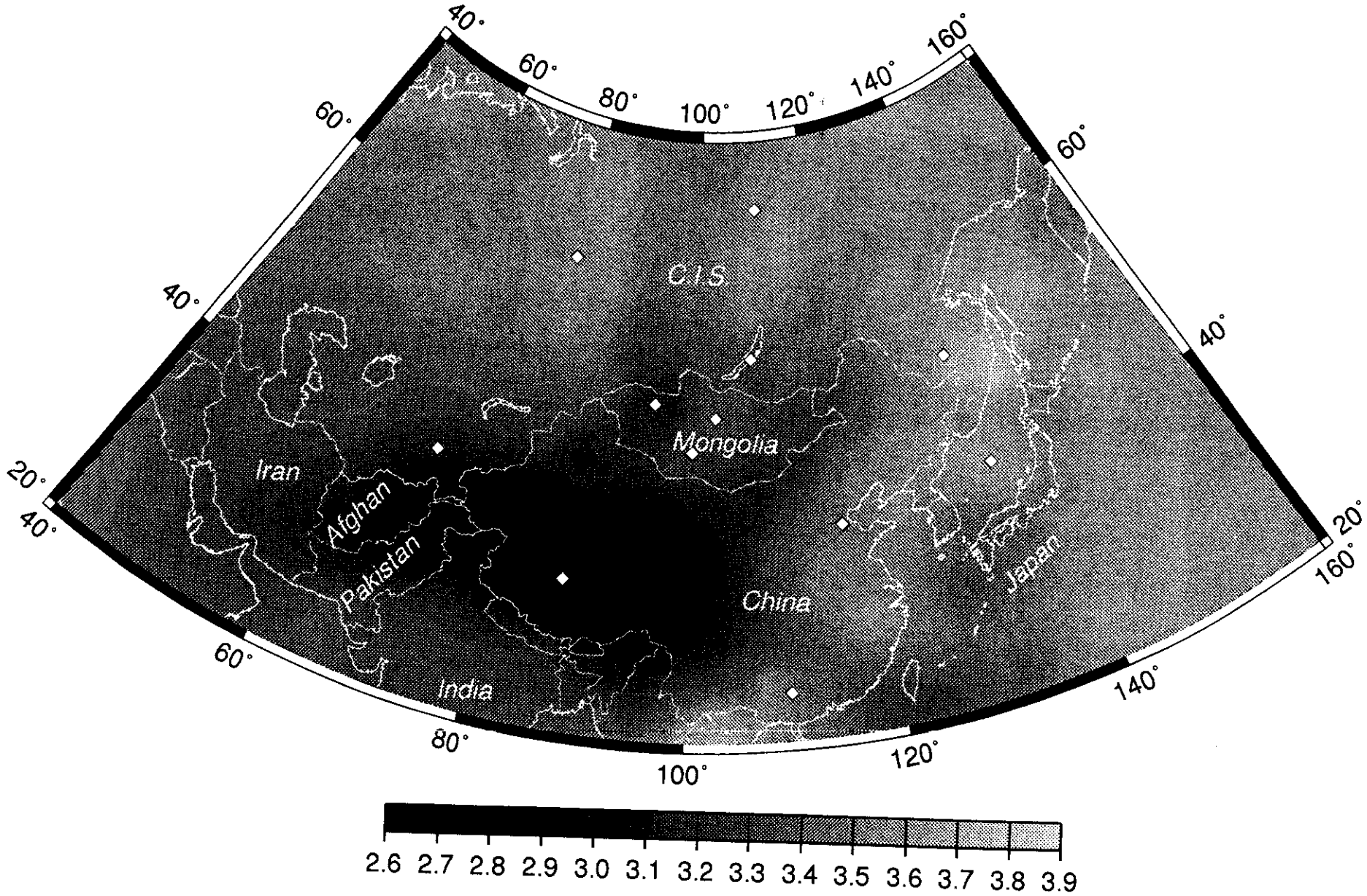
40°
60°
80°
100°
120°
140°
160°
20°
C.I.S
Mongolia
Iran
Afghan
Pakistan
China
Japan
India
2.6 2.7 2.8 2.9 3.0 3.1 3.2 3.3 3.4 3.5 3.6 3.7 3.8 3.9

Fig 4b

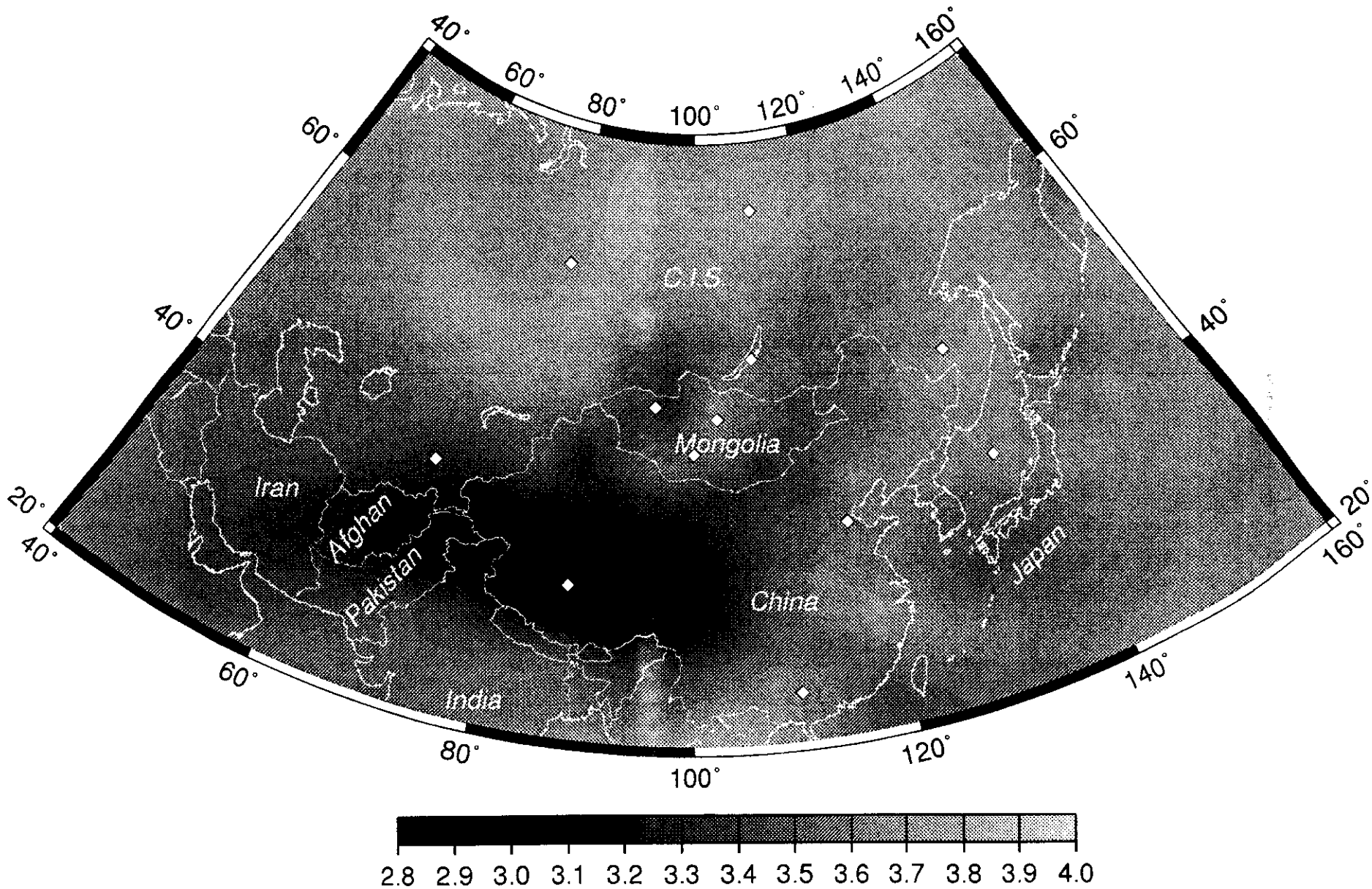
40°
60°
80°
100°
120°
140°
160°
20°
C.I.S.
Mongolia
Iran
Afghan
Pakistan
China
India
Japan
2.8 2.9 3.0 3.1 3.2 3.3 3.4 3.5 3.6 3.7 3.8 3.9 4.0

Fig 4c

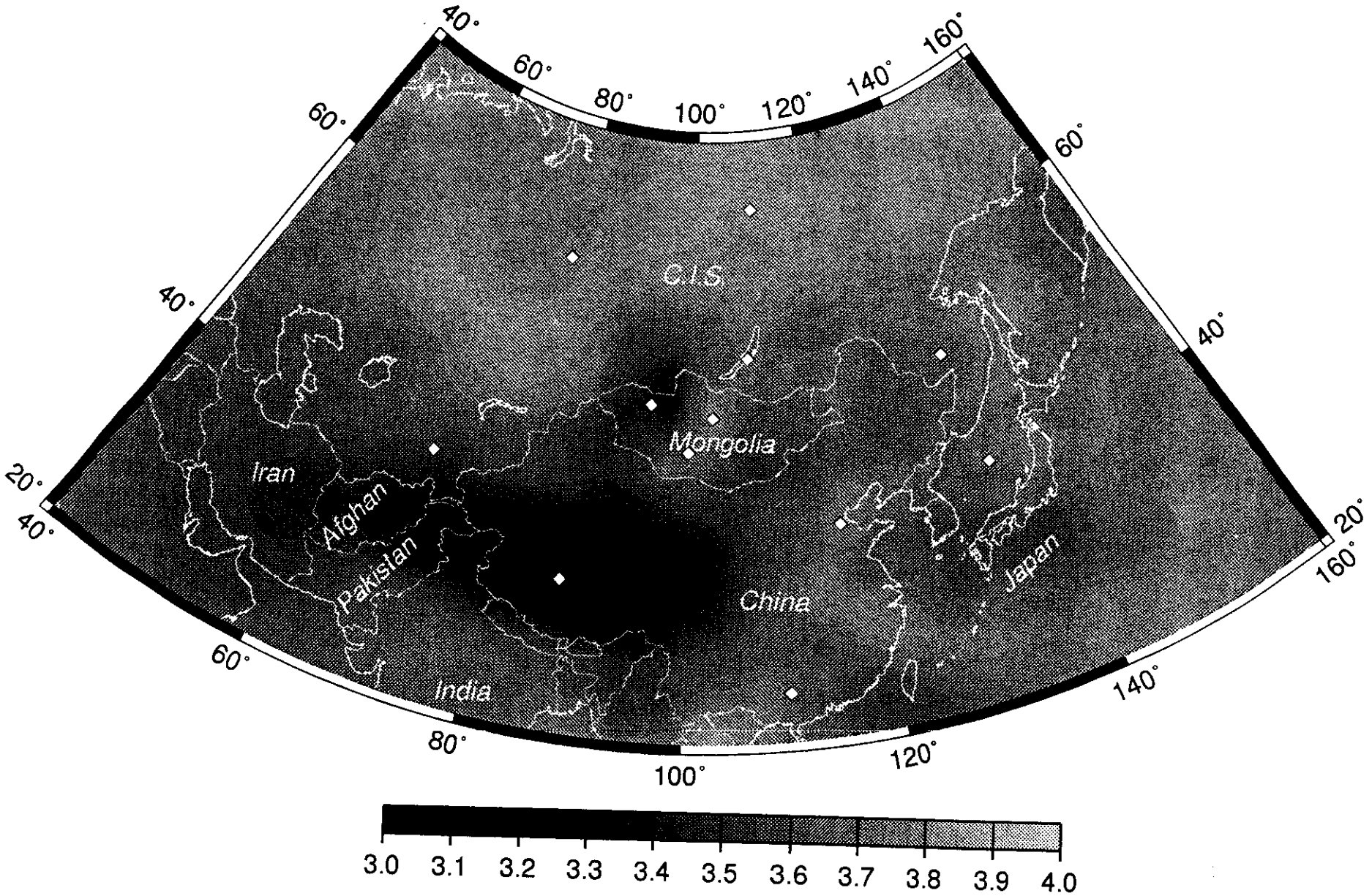
40°
60°
80°
100°
120°
140°
160°
20°
C.I.S.
Mongolia
Iran
Afghan
Pakistan
China
India
Japan
3.0
3.1
3.2
3.3
3.4
3.5
3.6
3.7
3.8
3.9
4.0

Fig 4d

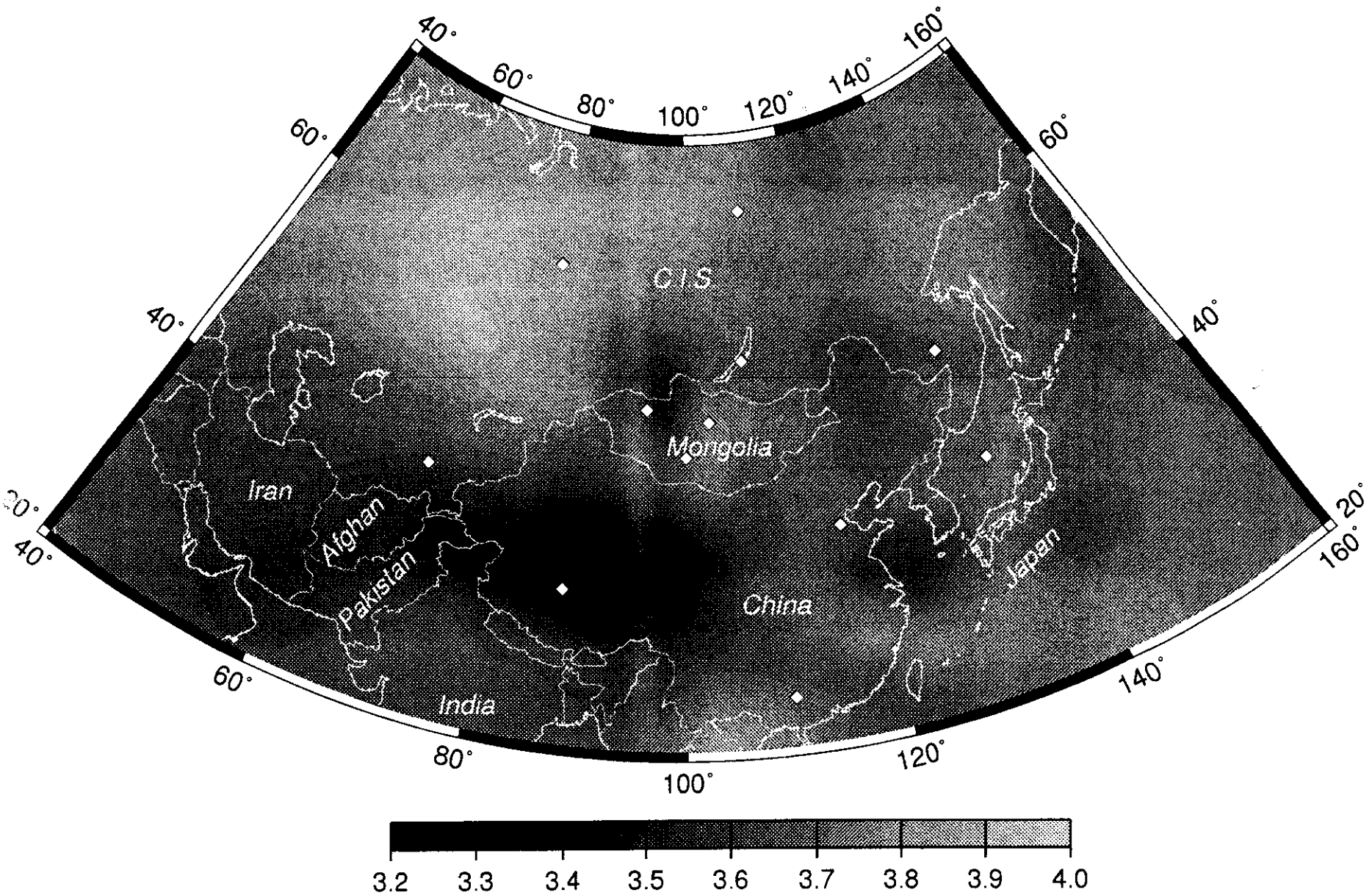
40°
60°
80°
100°
120°
140°
160°
20°
C.I.S.
Mongolia
Iran
Afghan
Pakistan
India
China
Japan
3.2
3.3
3.4
3.5
3.6
3.7
3.8
3.9
4.0

Fig 4e

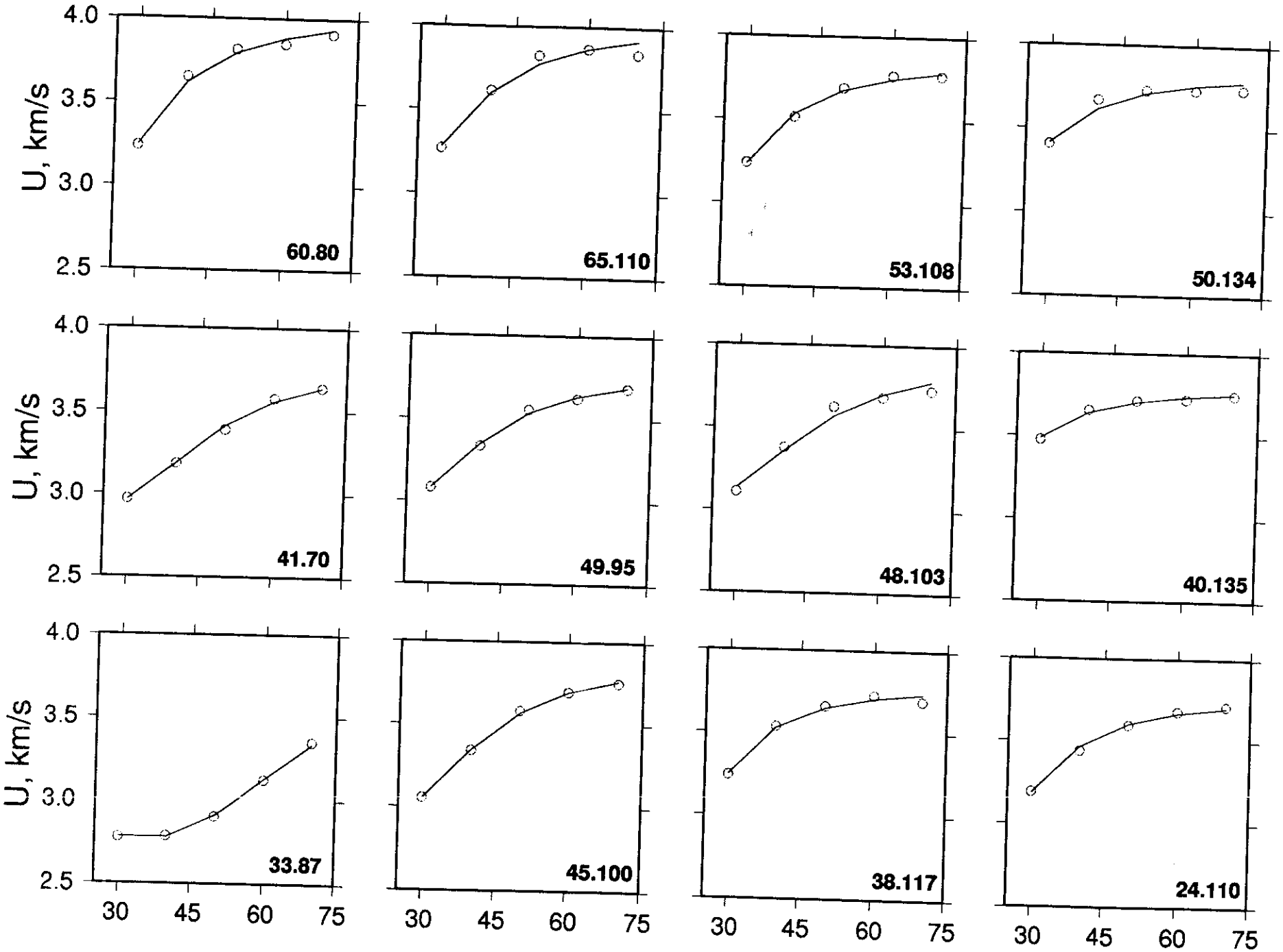
4.0
3.5
3.0
2.5
U, km/s
60.80
65.110
53.108
50.134
41.70
49.95
48.103
40.135
33.87
45.100
38.117
24.110
30
45
60
75
Period, Sec

Fig 5

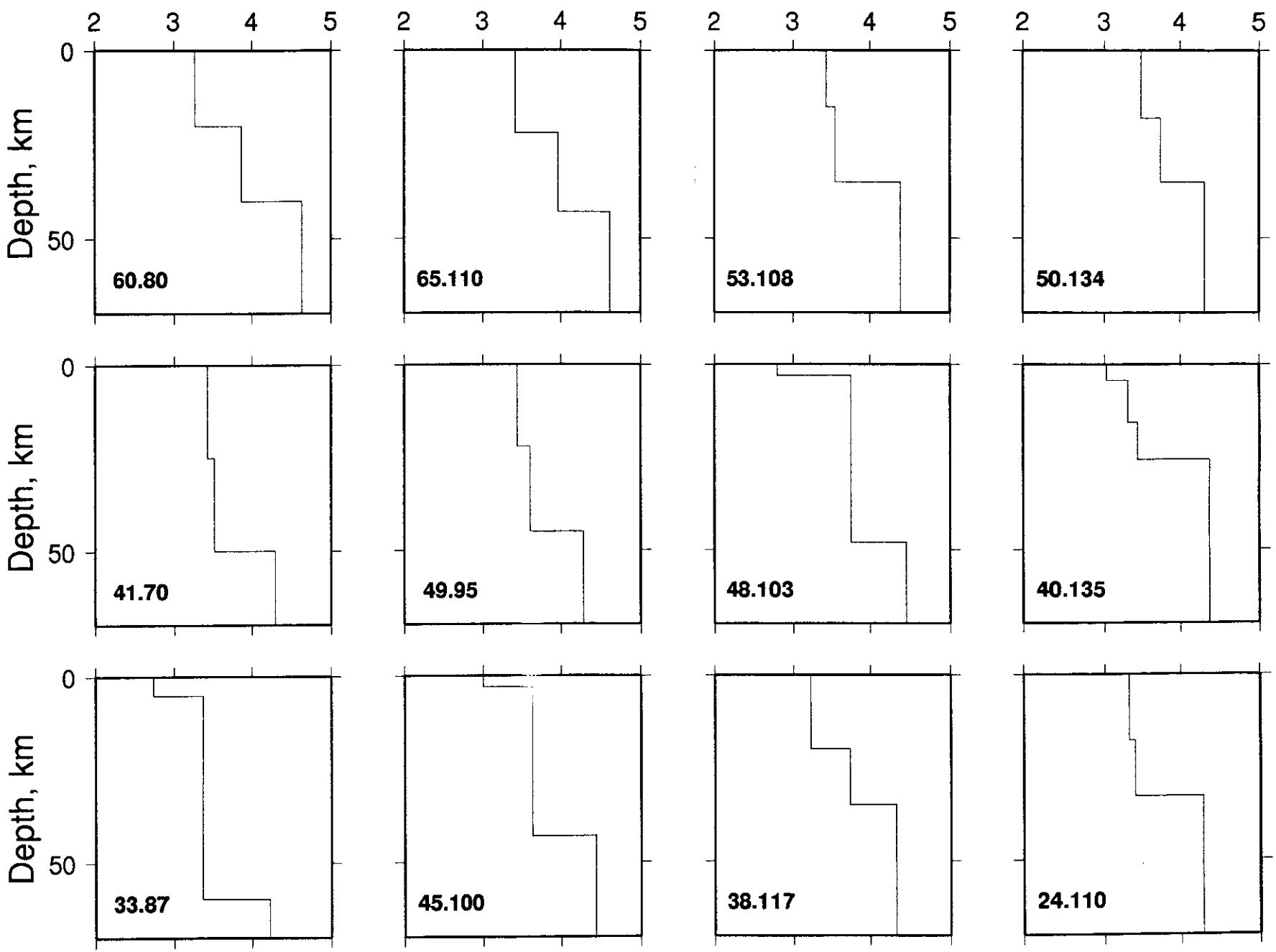
S Velocity, Km/s
2
3
4
5
0
50
Depth, km
60.80
65.110
53.108
50.134
41.70
49.95
48.103
40.135
33.87
45.100
38.117
24.110

Fig 6

Hobsogol rift and the western end of the Tunka rift; this establishes a triple junction (Yarmolyuk et al., 1990).

Current data suggest that the rifts of the Mongolian plateau formed at different times since the Oligocene and that they are at different stages of development.

Active strike-slip faults, notably the east-trending Bolnai fault, slice the Mongolian plateau (Tapponnier and Molnar, 1979). Some of these faults may be transfer zones between rifts. Others are more regional features and may be long-distance expressions of the India-Asia collision.

Basaltic Volcanism

Since the Miocene the Mongolian plateau has been the focus of intense basaltic volcanism (Figs. 2 and 3) that has within-plate characteristics; it was described as hotspot volcanism by Şengör (1987, Fig. 10) and as a hot field in the mantle by Zonenshain et al. (1991). There was a change from dominantly transitional-alkali magmatism in the Miocene to distinctly alkaline in the Pliocene and Quaternary (Genshaft and Saltykovskiy, 1987). Characteristic features of this late Cenozoic magmatism are the high potassium content and high K/Na ratio of the basaltic rocks. Ages are based on Russian K-Ar dates (Whitford-Stark, 1987). Spinel lherzolite xenoliths in alkali basalts from Hangai were most likely transported by a mantle diapir (Stosch et al., 1986).

Miocene, Pliocene, and Quaternary volcanic centers are located in the Baikal rift and in associated rifts to the northeast, but larger basaltic fields cover a wide plateau region on the eastern flank of this rift zone. This association of volcanism in both rifts and on rift flanks also exists in the Mongolian rifts. In the Tunka depression, volcanic rocks in the form of flows and cones up to 600 m thick range in age from Paleocene to Holocene. An extensive belt of volcanic rocks is associated with the Hangai dome and forms both lava fields and cone-shaped volcanoes dated and grouped as Eocene, Miocene, Pliocene–early Pleistocene, and Quaternary. In the Hobsogol rift region, basalts dated as Pliocene to Quaternary (the youngest are 4 ka) form large flows and are the remnants of a single volcanic plateau (Whitford-Stark, 1987).

The basaltic volcanism of the Mongolian plateau is concentrated in those regions (e.g., Baikal, Tunka, Hangai) where the heat flow is highest, the lithosphere is thinnest, and the rifts are well developed.

Thrusts

An interesting but problematic feature of the Mongolian plateau is the presence of Cenozoic thrusts (Fig. 1): there are not many and there is no published synthesis of them. Nevertheless, from data in Ufimtsev (1990) and Ruzhich et al. (1972), it seems likely that several thrusts are situated on or near the margins of the plateau and dip inward toward the plateau's interior. They are found on the west side of Baikal, north of Tunka, on the south side of the Hangai dome, and to the southeast of the Hentai dome. According to G. F. Ufimtsev (1991, personal commun.), many thrusts must be of Holocene age because they affect the present topography. North of the Tunka rift several east-striking Cenozoic thrusts have deformed and displaced basaltic dikes, one of which has three K/Ar ages ranging from 9.9 to 14.4 Ma (Ruzhich et al., 1972). We speculate that the uplifted plateau is in a state of collapse, not only by rifting but also by thrusting at its margins. Small Neogene and Quaternary molasse basins, situated adjacent to some thrusts around the margins of the plateau, may be incipient foreland basins.

PLUME MODEL

Although rifts, high heat flow, and alkaline basaltic magmatism are all signatures of lithospheric extension, other features of the Mongolian plateau are not consistent with an origin as a split in the Asian land mass generated by the India-Asia collision (Tapponnier et al., 1986). (1) The plateau's uplift is inconsistent with lithospheric thinning above normal asthenosphere (e.g., Dewey, 1982). For example, the Shansi grabens of northeast China (which have also been interpreted as the result of lithospheric cracking north of the Indian indenter) form a topographically low region. (2) The alkalic magmatism and high heat flow are not confined to the localized rifts, but extend across the plateau. This implies a laterally extensive heat source. (3) There is no single, dominant rift orientation. The Oka-Hobsogol-Tunka triple junction suggests local control by domal uplift. This is not consistent with a model of east-west extension generated by north-south compression across Asia.

The initial stages of mantle plume–continental lithosphere interaction are poorly known, but uplift, basic alkaline magmatism, high heat flow, and lithospheric thinning are characteristic signatures. The geological and geophysical data outlined above for the Mongolian plateau match these known plume-generated features, and thus we are in agreement with Logatchev et al. (1983), Logatchev and Zorin (1987), Khain (1990), Yarmolyuk et al. (1990), and Bal-

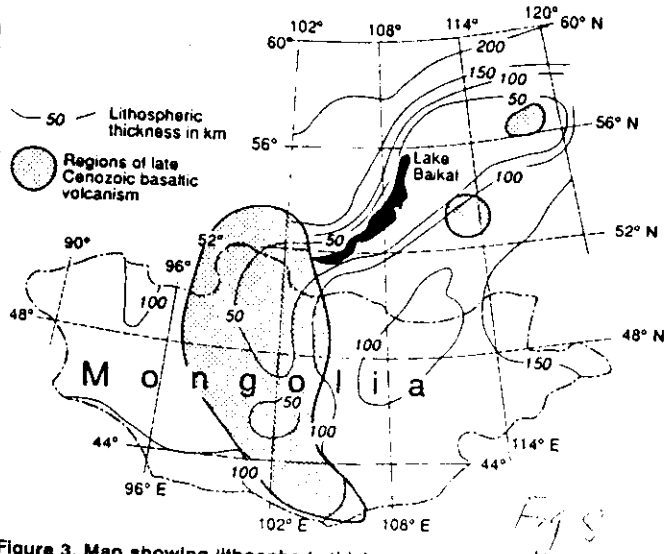

Figure 3. Map showing lithospheric thickness of Mongolian plateau and correlation with main region of late Cenozoic basaltic volcanism (after Zorin et al., 1990).

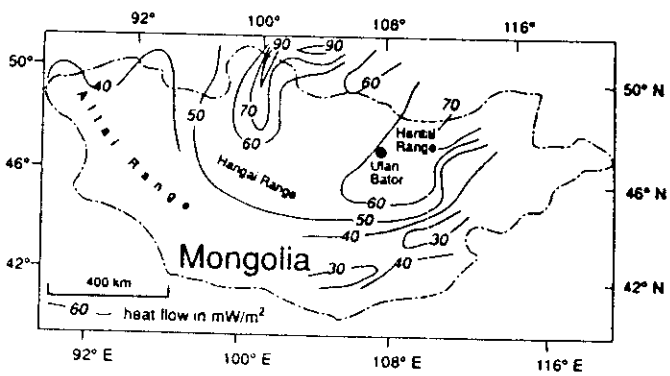

Figure 4. Heat-flow map of Mongolian plateau (after Khutorskoy and Yarmoiuk, 1989). Value of 120 mW/m² is recorded in Lake Hobsogol within 90 mW/m² contour in northern Mongolia.